Filtered OFDM Systems, Algorithms and Performance Analysis for 5G and Beyond

Lei Zhang, Ayesha Ijaz, Pei Xiao, Mehdi Molu and Rahim Tafazolli

***Abstract*—Filtered orthogonal frequency division multiplexing (F-OFDM) system is a promising waveform for 5G and beyond to enable multi-service system and spectrum efficient network slicing. However, the performance for F-OFDM systems has not been systematically analyzed in literature. In this paper, we first establish a mathematical model for F-OFDM system and derive the conditions to achieve the interference-free one-tap channel equalization. In the practical cases (e.g., insufficient guard interval, asynchronous transmission, etc.), the analytical expressions for inter-symbol-interference (ISI), inter-carrier-interference (ICI) and adjacent-carrier-interference (ACI) are derived, where the last term is considered as one of the key factors for asynchronous transmissions. Based on the framework, an optimal power compensation matrix is derived to make all of the subcarriers having the same ergodic performance. Another key contribution of the paper is that we propose a multi-rate F-OFDM system to enable low complexity low cost communication scenarios such as narrow band Internet of Things (IoT), at the cost of generating inter-subband-interference (ISubBI). Low computational complexity algorithms are proposed to cancel the ISubBI. The result shows that the derived analytical expressions match the simulation results, and the proposed ISubBI cancelation algorithms can significantly save the original F-OFDM complexity (up to 100 times) without significant performance loss.**

***Index Terms*—Filtered OFDM, inter-subband-interference, adjacent-carrier-interference, asynchronous system, multi-rate, waveform, network slicing, NB-IoT**

I. Introduction

Enhanced mobile broadband (eMBB), massive machine type communications (mMTC) and ultra-reliable and low latency communications (URLLC), have been categorized as three main communication scenarios for the 5-th Generation (5G) wireless communication [1], [2], [3]. In order to efficiently support the diverse requirements of 5G and spectrum efficient network slicing, from the physical layer perspective, one of the fundamental and key challenges over the previous systems, e.g., orthogonal frequency division multiplexing (OFDM) based long term evolution (LTE) [4], is the new waveform design to enable the multi-service signal multiplexing and isolation [5]. Besides inheriting the advantages of the OFDM systems, such as ease of implementation of channel estimation/equalization and multi-antenna techniques, there are two imperative features that the new waveform must possess to sustain the overall design requirements of 5G: low out of band emission (OoBE) and relaxed synchronization requirements. The first one may reduce guard band (e.g. 10% in OFDM based LTE) to a much smaller value (e.g., 2%) to achieve spectrum efficient transmissions [6]. In addition, this feature also provides a foundation for enabling multiple types of services with different optimal frame structures co-existing in one baseband with negligible interference [5], [7]. On the other hand, relaxed synchronization can lead to simplified hardware/algorithm design and transceiver processing [8]. For example, low complexity low cost MTC devices may not have sophisticated RF hardware and/or baseband synchronization algorithms [3], [9], [10]; in addition, asynchronous transmission may be adopted in 5G for uplink transmission to save the synchronization signaling overhead (e.g., timing advance in LTE uplink transmission) in mMTC scenarios.

Many waveforms have been proposed to meet (or partly meet) these design metrics and requirements, such as filter-bank multi-carrier (FBMC) [11], [12], [13], generalized frequency division multiplexing (GFDM) [14], [15], universal filtered multi-carrier (UFMC) [16], [5], [17], filtered orthogonal frequency division multiplexing (F-OFDM) [7], [18] and their variants [19], [20], [21], [22], [23]. Among them, FBMC system offers the best OoBE and time/frequency localization properties. However, channel estimation/equalization and its combination with multi-antennas system may be significantly more complex than OFDM due to the intrinsic interference between the real and imaginary branches [11], [24]. Recently, the authors in [25] proposed a low complexity one-tap channel equalization algorithm with additional cyclic prefix (CP) insertion to the original FBMC system [25]. In addition, for low-to-middle frequency selectivity channels, [26] proposed block-wise Alamouti schemes for FBMC systems with complex orthogonality. Like FBMC, GFDM is also a per-subcarrier filtered and block-based-processing system that may not be applicable to the latency sensitive services (e.g., vehicle to vehicle). Both UFMC system and F-OFDM are per subband filtered and symbol-based-processing waveforms. One of the major differences between them is that UFMC uses short filter (e.g., Chebyshev filter with length similar to channel length [16], [5]) and the filter tail does not extend to the next symbol at the transmitter. Whereas, F-OFDM normally adopts much longer filter (e.g., windowed Sinc filter with length being half of the symbol duration [7]). However, the filter tails (typically totally) extend to the adjacent symbols to keep the system overhead the same as the CP OFDM system (e.g., 7%) [7], [18]. This overlapping may make the system incur more inter-symbol-interference (ISI) and/or inter-carrier-interference (ICI) than the UFMC system in a scenario wherein a subband occupies small percentage of the

Lei Zhang is with School of Engineering, University of Glasgow, Glasgow, G12 8QQ, U.K. Ayesha Ijaz, Pei Xiao, Mehdi Molu and Rahim Tafazolli are with the 5G Innovation Centre (5GIC) and Institute for Communication Systems (ICS), University of Surrey, Guildford, GU2 7XH, UK (Email: lei.zhang@glasgow.ac.uk).

whole bandwidth (e.g., 1%) [2]. However, the longer filter and soft overlapping among adjacent symbols in F-OFDM render the system much more robust to the adjacent-carrier-interference (ACI) and the multiple-access-interference (MAI) in the asynchronous systems (for uplink). Since this is one of the main targets and a challenging communication scenarios for 5G from the physical layer perspective, our performance analysis and proposed algorithms in this paper will be focused on the F-OFDM system only. However, the basic idea could be extended to other waveforms such as UFMC.

As mentioned above, F-OFDM uses filter with length up to half of the symbol duration for good frequency localization. This design criterion may make the system vulnerable to ISI and ICI. Most of the existing work on F-OFDM, found in the literature, is focused on the numerical comparisons with other waveforms and sensitivity to the synchronization errors [7], [27], [18], [28]. Some conclusions are made based on specific simulation setups or qualitative analysis. However, a systematic analysis on the performance in terms of ISI, ICI and ACI is missing. For instance, it has been claimed that increasing the CP length may reduce interference in F-OFDM [7], [18]. However, maximum CP length required to limit the interference level is unknown. This is a critical issue for the 5G system design and it is one of the questions answered in this paper. It is a common problem in the subband filtered system that the power is not evenly allocated to each subcarrier due to the filter ramping-up and ramping-down at the edges of a subband [5]. Based on our framework, we derive a power compensation matrix to compensate the power among subcarriers in order to output the same signal-to-noise-ratio (SNR) for optimal performance. In addition, an updated one-tap channel equalizer is proposed by considering all of the above mentioned imperfections and power compensation.

In addition to the tradeoff between overhead and performance, the tradeoff between complexity and performance is another important consideration in the system design. In the original F-OFDM system with small subband bandwidth (e.g., 12 subcarriers as a subband) to support multiple users/services, each subband may require an independent Discrete Fourier Transform (DFT) or fast Fourier transform (FFT) operation, which may result in more than 100 times higher complexity than the OFDM system (assuming the system has more than 100 subbands) at the base station. The complexity issue is also a major challenge for low cost low complexity devices (e.g., internet of things (IoT) devices), where narrow band IoT has been proposed as a promising solution for 5G system to balance the performance and system implementation complexity [3], [10], [29]. However, with the original F-OFDM system, the FFT size and sampling rate should be kept as high as the normal user devices to secure the orthogonality among subbands, which may be against the design principles for low complexity low cost devices.

As a solution, in this paper, we propose multi-rate F-OFDM for computational complexity reduction. In the single-rate (SR) F-OFDM system, the baseband sampling rate is fixed and kept the same for all subbands. On the contrary, multi-rate (MR) F-OFDM has variable sampling rate in the baseband signal processing to use low complexity low-dimension DFT. However, MR processing creates image signals in adjacent bands and anti-image subband filters are required to eliminate the image signals [27]. Nevertheless, the residual image signal will create ISubBI in the system due to non-ideal filters, which may degrade system performance in comparison with the SR. To deal with the problem, we propose low-complexity baseband signal processing algorithms to precancel the ISubBI by precoding the information symbols for downlink transmission. The idea can be also extended to the uplink transmission by jointly detecting the receiver signals. Note that the concept of MR implementation of multi-service subband filter multi-carrier (SFMC) has been proposed in [27], however, it was focused on the system model and simulation comparisons only.

Two main contributions and novelties of this paper are summarized as follows:

- We first build an analytical framework for F-OFDM system by considering the ISI, ICI and ACI in asynchronous systems. The conditions to achieve interference free transmission and one-tap channel equalization are derived for F-OFDM. In the practical cases (e.g., insufficient CP length and asynchronous transmission, etc.), the analytical expressions of ISI, ICI and ACI are derived, which provide a guideline for 5G frame structure and waveform design. Based on the analytical framework, the optimal power compensation matrix is derived to make the subcarriers in a subband have the same performance in terms of SNR. In addition, we propose channel equalization algorithms by taking the derived interference and power compensation into consideration.
- We systematically establish a system model for MR F-OFDM and propose low complexity ISubBI cancelation algorithms by taking downlink transmissions as an example. The channel dependent and independent algorithms are proposed. The algorithms are flexible to support arbitrary bandwidth interference cancelation. For downlink transmission, preprocessing is applicable at the base station to pre-cancel the interference. For the uplink transmission, joint detection at the receiver side can be performed to mitigate the ISubBI and improve the performance. The proposed scheme and interference cancelation algorithm can provide a viable solution for low complexity IoT/MTC devices.

Notations: Vectors and matrices are denoted by lowercase and uppercase bold letters, and $\{\cdot\}^H, \{\cdot\}^T, \{\cdot\}^*$ stand for the Hermitian conjugate, transpose and conjugate operation, respectively. We use trace$\{\mathbf{A}\}$ and diag$\{\mathbf{A}\}$ to denote the trace of matrix $\mathbf{A}$ and a diagonal matrix formed by taking the diagonal elements of $\mathbf{A}$, respectively. However, diag$\{\mathbf{a}\}$ denotes forming a diagonal matrix $\mathbf{A}$ using the vector $\mathbf{a}$. $\mathbf{I}_M$ and $\mathbf{0}_{m\times n}$ refer to $M \times M$ identity matrix and $m \times n$ zero matrix, respectively. Operator $*$ denotes linear convolution of two vectors. $A(i, j)$ means taking the i-th row and j-th column of the matrix $\mathbf{A}$. $\uparrow K$ and $\downarrow K$ refer the operation of up-sampling and down-sampling the signal by a factor of K, respectively.

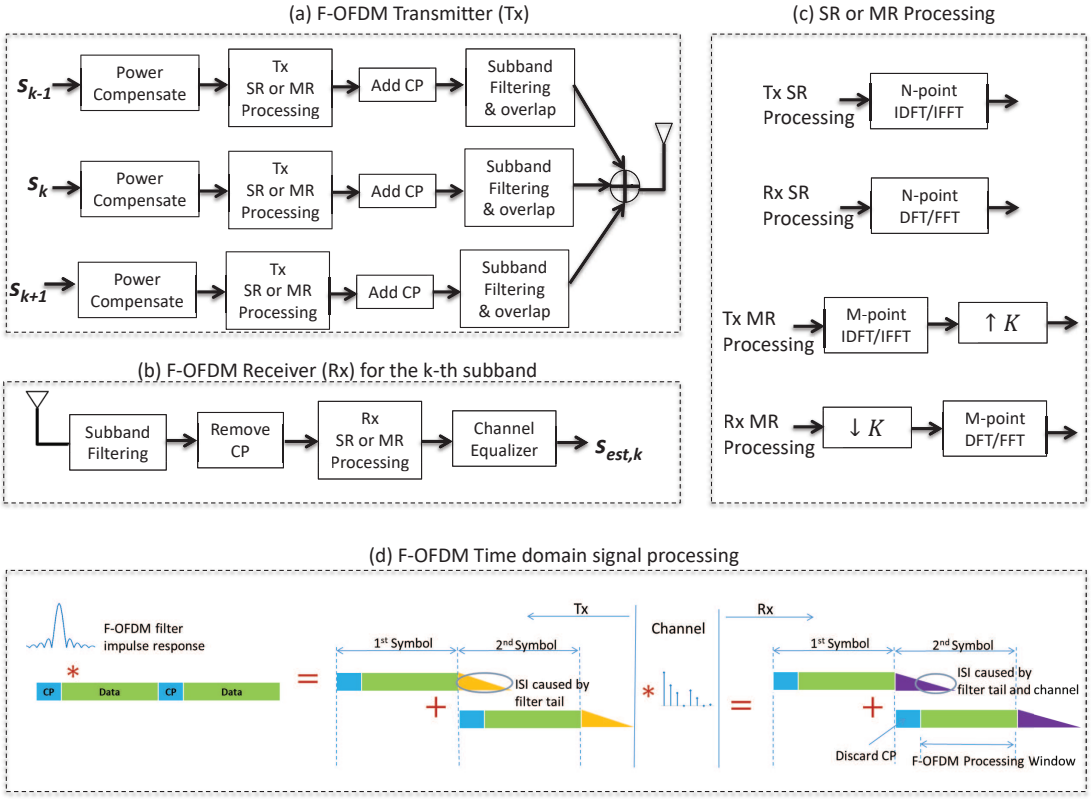

Fig. 1. Block diagram of SR and MR F-OFDM systems (We consider 3 contiguous subbands in the frequency domain and 2 symbols in the time domain in this diagram for brevity).

II. Single-rate F-OFDM System

A downlink SR F-OFDM system is shown in Fig. 1, a power compensation is operated on each subband signal to compensate the filter frequency response difference among subcarriers. A normal CP-OFDM process is implemented on per subband basis. Then a subband filter is followed with the output data length being altered due to the filter tails. However, the tail of the current symbol overlaps with the next symbol (see Fig. 1 (d)) and therefore, does not cause extra overhead. The subband filter takes the role of isolating the interference from the adjacent subbands and reducing the OoBE. At the receiver side, as shown in Fig. 1 (b), an optional matched filter is used followed by CP removal and DFT or FFT processing. Note that Fig. 1 is a downlink transmission system. The uplink transmission system uses reverse procedure with an optional DFT spreading on the modulated symbols for peak-to-average-power-ratio (PAPR) reduction. However, to focus on the interference analysis and cancelation algorithms, we will not consider the PAPR reduction algorithms (e.g., DFT spreading processing) in this paper.

A. Transmitter Processing

Let us consider an F-OFDM system contains N subcarriers that are divided into K subbands with each subband transmitting M contiguous subcarriers, i.e., $N = M \cdot K$ [1]. Writing the transmitted symbols in vector form:

$$\mathbf{s} = [\mathbf{s}_1; \mathbf{s}_2; \cdots; \mathbf{s}_K] \in \mathbb{C}^{N\times 1}, \tag{1}$$

where

$$\mathbf{s}_k = [s_k(1), s_k(2), \cdots, s_k(M)]^T \in \mathbb{C}^{M\times 1} \tag{2}$$

is the signal transmitted in the k-th subband. We assume $\mathcal{E}\{|s_k(i)|^2\} = \rho^2_{sym}$, for $i = 0, 1, \cdots, N-1$. Generally, multiple subbands can be assigned to one user [5]. However, to simplify the derivations and without loss of generality, we assume that each user has been assigned a single subband, i.e., the k-th subband is allocated to the k-th user [2]. We can write the transmitted signal *before* subband filtering for the k-th subband as $\mathbf{R}\mathbf{D}_k\mathbf{E}_k\mathbf{s}_k$, where $\mathbf{R} = [\mathbf{0}_{L_{CP}\times(N-L_{CP})}, \mathbf{I}_{L_{CP}}; \mathbf{I}_N]$ is the matrix form of CP insertion operation, with L_{CP} being the CP length and $L_{SYM} = N + L_{CP}$ being the symbol duration in F-OFDM samples. $\mathbf{D}_k \in \mathbb{C}^{N\times M}$ is the $[(k-1)M+1]$-th to the (kM)-th columns of the N-point normalized inverse DFT (IDFT) matrix $\mathbf{D}$. The element of $\mathbf{D}$ in the i-th row and n-th column is $D(i,n) = \frac{1}{\sqrt{N}} e^{j\cdot 2\pi in/N}$.

As mentioned early, power compensation processing matrix $\mathbf{E}_k \in \mathbb{R}^{M\times M}$ can be adopted so that all subcarriers have the same ergodic output SNR to compensate the filter frequency selectivity on different subcarriers. Note that the value of $\mathbf{E}_k$

[1]This equation implies that all of the N consecutive subcarriers are occupied. Otherwise, the transmitted symbols can be set to zero at the unoccupied subcarriers to satisfy the assumption.

[2]Note that assigning multiple subbands to a single user is a special case of single subband assignment, since in the latter case, we can always set several subbands' configurations the same to each other and with no synchronization error among the subbands, which will be equivalent to the multiple subbands assignment case.

depends on the filter frequency response and the optimal value will be given in Section III-C and when $\mathbf{E}_k = \mathbf{I}_M$, no power compensation is applied to the system.

Let us assume that the k-th subband filter impulse response is

$$\mathbf{a}_k = [a_k(0), a_k(1), \cdots, a_k(L_F-1)] , \quad (3)$$

with L_F being the filter length. In addition, we assume all subbands use the same prototype filter (e.g., same filter length and type) and we assume that the energy of $\mathbf{a}_k$ is normalized to unity, i.e., $\sum_{l=0}^{L_F-1} |a_k(l)|^2 = 1$. However, these assumptions can be easily removed without affecting the algorithms and analysis results. In order to express the system model into a matrix operation form, let us define an $(L_{SYM}+L_F-1)\times L_{SYM}$ dimension Toeplitz matrix $\mathbf{A}_k$ with its first column being $[\mathbf{a}_k, \mathbf{0}_{1\times(L_{SYM}-1)}]^T$ and first row being $[a_k(0), \mathbf{0}_{1\times(L_{SYM}-1)}]$. We can write the transmitted signal after subband filtering for the k-th subband as $\mathbf{A}_k\mathbf{R}\mathbf{D}_k\mathbf{E}_k\mathbf{s}_k$. Note that the number of overall samples that contains the desired signal is $L_{SYM}+L_F-1$ due to the filter tails.

After filter tail overlapping processing (as shown in Fig. 1 (d)), the current symbol at the k-th subband will be overlapped with one previous and one next symbol [3]. In this case, we can write the k-th subband signal before transmission as

$$\mathbf{q}_k = \frac{1}{\rho_k}[\hat{\mathbf{q}}_{DES,k} + \hat{\mathbf{q}}_{ISI,k}] , \quad (4)$$

where the first term $\hat{\mathbf{q}}_{DES,k} = \mathbf{A}_k\mathbf{R}\mathbf{D}_k\mathbf{E}_k\mathbf{s}_k$ is the desired signal. The second term is the ISI due to the filter tail overlapping with the previous and next symbol, which will be analyzed in detail in the next section. ρ_k is the transmission power normalization factor of the k-th subband.

B. Receiver Processing

Let us assume the channel impulse response between the transmitter and the k-th user is $\mathbf{b}_k = [b_k(0), b_k(1), \cdots, b_k(L_{CH,k}-1)]$ where $L_{CH,k}$ is the length of the channel in F-OFDM samples [4]. We assume that different taps of the channel are uncorrelated, i.e., $\mathcal{E}\{b_k(i)b_k(l)^*\} = 0$ if $i \neq l$ and $\mathcal{E}\{b_k(i)b_k(l)^*\} = R_k(i)$ if $i = l$.

Without loss of generality, we assume the overall channel gain for the k-th user is $\sum_{i=0}^{L_{CH,k}-1} \mathcal{E}$ $|b_k(i)|^2 = \rho^2_{CH,k}$. Let us define $\mathbf{B}_{all,k} \in \mathbb{C}^{(L_{SYM}+L_{CH,k}+L_F-2)\times(L_{SYM}+L_F-1)}$ as the equivalent channel convolution Toeplitz matrix of $\mathbf{b}_k$ with its first row being $[b_k(1), \mathbf{0}_{1\times L_{SYM}+L_F-2}]$ and first column is $[\mathbf{b}_k, \mathbf{0}_{1\times L_{SYM}+L_F-L_{CH,k}-2}]^T$.

At the receiver, due to the filter tails and channel dispersion, in total $L_{SYM}+L_{CH,k}+L_F-2$ samples contains the desired signal. How to select the receiver processing window (i.e., L_{SYM} out of $L_{SYM}+L_{CH,k}+L_F-2$ samples) is critical to mitigate the ISI. In general, a shift of L_s samples from the first sample that contains the desired signal could be selected to balance the ISI between the previous and next symbols in the k-th subband. In this case, the current symbol might overlap with two adjacent symbols. Therefore, $\mathbf{B}_{all,k}$ can be split into three parts with the first part $\mathbf{B}_k^{UP}$ by taking its first L_s rows and the second part takes from the L_s+1-th to the L_s+L_{SYM} rows as $\mathbf{B}_k$ and the third part by taking its last $L_{CH,k}+L_F-2-L_s$ rows as $\mathbf{B}_k^{DW}$. The second part $\mathbf{B}_k$ will be the main part of channel matrix that convoluted with the signal for the desired signal detection, while $\mathbf{B}_k^{UP}$ and $\mathbf{B}_k^{DW}$ are the two parts which may generate ISI from the previous and next symbols, respectively.

Taking the linear receiver filtering, CP removal and DFT processing one by one, let us write the received signal at the k-th user as:

$$\mathbf{y}_k = \mathbf{y}_{DES,k} + \mathbf{y}_{ISI,k} + \mathbf{y}_{ACI,k} + \tilde{\mathbf{v}}_k . \quad (5)$$

The first term

$$\begin{aligned}\mathbf{y}_{DES,k} &= \mathbf{D}_k^H\mathbf{T}\mathbf{C}_k\mathbf{B}_k\mathbf{q}_{DES,k} \\ &= \frac{1}{\rho_k}\mathbf{D}_k^H\mathbf{T}\mathbf{C}_k\mathbf{B}_k\mathbf{A}_k\mathbf{R}\mathbf{D}_k\mathbf{E}_k\mathbf{s}_k \end{aligned} \quad (6)$$

is the term that contains the desired signal within the processing window. $\mathbf{C}_k$ is the matrix form of subband filter based on the receiver filter $\mathbf{c}_k = [c_k(0), c_k(1), \cdots, c_k(L_F-1)]$. In general, matched filter is employed, i.e., $\mathbf{C}_k = \mathbf{A}_k^H$. Without loss of generality, we assume the receiver filter length is the same as the transmitter filter's. The matrix $\mathbf{T} = [\mathbf{0}_{N\times L_{CP}}, \mathbf{I}_N]$ is matrix form of CP removal implementation. The ISI signal can be written as

$$\begin{aligned}\mathbf{y}_{ISI,k} &= \frac{1}{\rho_k}\mathbf{D}_k^H\mathbf{T}\mathbf{C}_k(\hat{\mathbf{B}}_k^{DW}\mathbf{A}_k\mathbf{R}\mathbf{D}_k\mathbf{E}_k\tilde{\mathbf{s}}_k \\ &+ \hat{\mathbf{B}}_k^{UP}\mathbf{A}_k\mathbf{R}\mathbf{D}_k\mathbf{E}_k\bar{\mathbf{s}}_k) , \end{aligned} \quad (7)$$

where $\hat{\mathbf{B}}_k^{DW} = [\mathbf{B}_k^{DW}; \mathbf{0}_{(L_{SYM}-L_{CH,k}-L_F+L_s+2)\times L_{SYM}}]$ and $\hat{\mathbf{B}}_k^{UP} = [\mathbf{0}_{(L_{SYM}-L_s)\times L_{SYM}}; \mathbf{B}_k^{UP}]$. $\tilde{\mathbf{s}}_k$ and $\bar{\mathbf{s}}_k$ are the transmitted symbols in the previous and next multicarrier symbol in the k-th subband.

The third term is the ACI in the k-th subband due to the non-orthogonality between subbands and the asynchronousity between the subbands. Since the k-th subband/user can overlap with up to three symbols in the i-th subband/user, let us define the three symbols with the i-th subband as: the previous one is $\mathbf{q}_i^U$, the middle as $\mathbf{q}_i^M$ and the latter is $\mathbf{q}_i^D$. Similarly, $\mathbf{B}_k^U$, $\mathbf{B}_k^M$ and $\mathbf{B}_k^D$ are three parts of the channel convolution matrix of $\mathbf{B}_k$. Specifically, $\mathbf{B}_k^U$ takes the first $L_s+\tau_i$ rows of $\mathbf{B}_{all,k}$; $\mathbf{B}_k^U$ takes the $L_s+\tau_i+1$-th to the $L_s+\tau_i+L_{SYM}$-th rows of $\mathbf{B}_{all,k}$; $\mathbf{B}_k^D$ takes the $L_s+\tau_i+L_{SYM}+1$-th to the $\tau_i+L_{SYM}+L_{CH,k}+L_F-2$-th rows of $\mathbf{B}_{all,k}$. Defining $\hat{\mathbf{B}}_k^D = [\mathbf{B}_k^D; \mathbf{0}_{(L_{SYM}-L_{CH,k}-L_F+L_s+\tau_i+2)\times L_{SYM}}]$ and $\hat{\mathbf{B}}_k^U = [\mathbf{0}_{(L_{SYM}-L_s-\tau_i)\times L_{SYM}}; \mathbf{B}_k^U]$, then we have

$$\mathbf{y}_{ACI,k} = \mathbf{D}_k^H\mathbf{T}\mathbf{C}_k \sum_{i=1, i\neq k}^{K} (\hat{\mathbf{B}}_k^U\mathbf{q}_i^D + \mathbf{B}_k^M\mathbf{q}_i^M + \hat{\mathbf{B}}_k^D\mathbf{q}_i^U) . \quad (8)$$

Due to the symbol overlapping, the ACI will not be zero even if the subbands are well synchronized (i.e., $\tau_i = 0$). However, in this case, the interference level could be significantly smaller.

[3]Note that this implies the filter length is no longer than a half of the symbol duration. Indeed, it is a common setup in literature to assume the filter length $L_F = N/2$.

[4]Note that we have assumed that each user is assigned to a single subband, therefore the channel from the base station to the k-th user is equivalent to the channel for the k-th subband.

Finally, $\tilde{\mathbf{v}}_k = \mathbf{T}\mathbf{C}_k\mathbf{v}_k$ is a complex-valued noise vector after receiver filtering for the k-th user and we assume $\mathbf{v}_k$ is white Gaussian noise with zero mean and variance σ^2.

III. Asynchronous F-OFDM System and Performance Analysis

In this section, we will consider the interference and noise terms in equation (5) and derive the analytical expressions one by one. The conditions for orthogonality and securing the circular convolution property between the channel and signal will be given in this section as well. In addition, a power compensation matrix will be derived so that all subcarriers in one subband have the same performance. Finally, based on the analytical results, we propose a modified channel equalizer by taking all of the interference into consideration.

A. Filter and Channel frequency response

Before we give any derivations, let us first define the filter and channel responses in frequency domain. We have defined $\mathbf{a}_k$, $\mathbf{c}_k$ and $\mathbf{b}_k$ as the subband filter at the transmitter, receiver and the channel impulse response, respectively. Let us define N dimension $\mathbf{f}_k$, $\mathbf{g}_k$ and $\mathbf{h}_k$ as the corresponding responses in frequency domain. Specifically

$$\begin{aligned}\mathbf{f}_k &= \mathbf{D}^H \cdot [\mathbf{a}_k, \mathbf{0}_{1\times(N-L_F)}]^T \,,\\ \mathbf{h}_k &= \mathbf{D}^H \cdot [\mathbf{b}_k, \mathbf{0}_{1\times(N-L_{CH,k})}]^T \,,\\ \mathbf{g}_k &= \mathbf{D}^H \cdot [\mathbf{c}_k, \mathbf{0}_{1\times(N-L_F)}]^T \,. \end{aligned} \tag{9}$$

Note that $\mathbf{f}_k$, $\mathbf{g}_k$ and $\mathbf{h}_k$ are $N\times 1$ vectors. Let us split the N elements into K parts, each containing M elements. Let $\mathbf{f}_k^{[i]}$, $\mathbf{g}_k^{[i]}$ and $\mathbf{h}_k^{[i]}$ be the i-th section of $\mathbf{f}_k$, $\mathbf{g}_k$ and $\mathbf{h}_k$, which consists of the $(i-1)M+1$ to the iM-th elements of $\mathbf{f}_k$, $\mathbf{g}_k$ and $\mathbf{h}_k$. Let us set three $M\times K$ matrices as:

$$\begin{aligned}\mathbf{F}_k &= [\mathbf{f}_k^{[1]}, \mathbf{f}_k^{[2]}, \cdots, \mathbf{f}_k^{[K]}] \,,\\ \mathbf{G}_k &= [\mathbf{g}_k^{[1]}, \mathbf{g}_k^{[2]}, \cdots, \mathbf{g}_k^{[K]}] \,,\\ \mathbf{H}_k &= [\mathbf{h}_k^{[1]}, \mathbf{h}_k^{[2]}, \cdots, \mathbf{h}_k^{[K]}] \,. \end{aligned} \tag{10}$$

Note that the value of $\mathbf{f}_k^{[i]}$ (and $\mathbf{g}_k^{[i]}$) is significantly larger for the k-th subband, i.e. for $i=k$, than for $i\neq k$. The values of $\mathbf{f}_k^{[i]}$ should be reduced exponentially when $|i-k|$ increases, i.e, the filter response of the k-th subband is significantly reduced in the subband that is away from the k-th subband. Therefore, the F-OFDM system provides much better OoBE and performance in the asynchronous cases.

An exemplary filter frequency response is shown in Fig. 2. For the first subband (red line), the filter passband response $\mathbf{f}_1^{[1]}$ (from 1st to 20-th subcarrier) has significantly larger values than the response in stopbands ($\mathbf{f}_1^{[2]}$, $\mathbf{f}_1^{[3]}$ and $\mathbf{f}_1^{[4]}$, i.e., from the 21-th to the 80-th subcarrier). On the other hand, the filter frequency response for the second subband (blue line) shifts its passband to the stopband of the first subband (i.e. the 21-th to the 40-th subcarrier). In this case, signals in the two subbands will be isolated by the subband filters without generating severe interference.

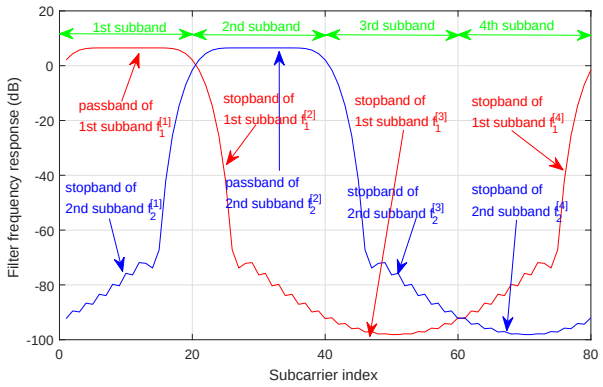

Fig. 2. Filter frequency response (FFR) versus subcarrier index ($N=80$; $M=20$; in total 4 subbands; only the first two subbands' FFR are given here. Subcarriers $1-20$ belong to the first subband, subcarriers $21-40$ belong to the second subband. Red and blue lines are the FFR for the first and second subbands, respectively. Windowed Sinc filter [7] with $L_F=41$.).

B. Interference-free F-OFDM system

Securing interference-free one-tap channel equalization is one of the most important design criteria in an multi-carrier system such as CP-OFDM, where CP with length equal to or longer than the channel dispersion in time domain is added to satisfy the circular convolution property between signal and channel, resulting in interference-free one-tap channel equalization. For F-OFDM system, we can also achieve the interference-free one-tap channel equalization at a cost of system overhead. By using $\bar{\mathbf{F}}_k^{[i]} = \text{diag}(\mathbf{f}_k^{[i]})$, $\bar{\mathbf{G}}_k^{[i]} = \text{diag}(\mathbf{g}_k^{[i]})$ and $\bar{\mathbf{H}}_k^{[i]} = \text{diag}(\mathbf{h}_k^{[i]})$, we have the following Proposition

Proposition 1: *Consider an F-OFDM system as shown in Fig. 1. The filter and channel response are defined in equation (9) and (10). The desired signal and the channel frequency response can be written as the following point-wise multiplications:*

$$\mathbf{y}_k = \frac{1}{\rho_k}\bar{\mathbf{G}}_k^{[k]}\bar{\mathbf{H}}_k^{[k]}\bar{\mathbf{F}}_k^{[k]}\mathbf{E}_k\mathbf{s}_k + \tilde{\mathbf{v}}_k \,, \tag{11}$$

if

$$L_{CP} \geq L_O \text{ and } 0 \leq \tau_i \leq L_{CP} - L_O \quad \text{for} \quad i = 1,\cdots,K \,, \tag{12}$$

where $L_O = L_{CH} + 2L_F - 3$ and $\tilde{\mathbf{v}}_k$ is Gaussian white noise after filtering with correlation matrix being $\sigma^2\mathbf{Q}_k$ and $\mathbf{Q}_k = \text{diag}[\mathbf{D}_k\mathbf{T}\mathbf{C}_k\mathbf{C}_k^T\mathbf{T}^H\mathbf{D}_k^H]$.

Proof: See Appendix A. ■

Equation (11) implies that interference-free one-tap equalization can be achieved in F-OFDM if equation (12) is met. However, the two conditions are hardly satisfied strictly due to the following reasons: 1), the filter length in F-OFDM is normally set much longer than the channel length to achieve good filter response and low OoBE and the typical value is half of the symbol duration [7], [18]. Designing a system with such long CP may not be spectrum efficient; 2), the system might be asynchronous in some communication scenarios such as mMTC uplink transmission.

C. The proposed power compensation matrix

According to the system model in (11), it is intuitive to understand that the SNR at different subcarriers in one subband could be different. Specifically, the power at the m-th subcarrier in the k-th subband can be written as $SNR_k(m) = \frac{\rho_{sym}^2\rho_{CH,k}^2}{\rho_k^2\sigma^2} \cdot |g_k^{[k]}(m)f_k^{[k]}(m)E_k(m,m)|^2/|Q_k(m,m)|^2$. In the original F-OFDM system, no power compensation is considered (e.g., $E_k(m,m) = 1$ for all m.). In this case, the SNR in subcarriers may not be the same for different m. Since each subcarrier carries information with the same importance, therefore, it is beneficial to design the power compensation matrix to ensure that each subcarrier has the same detection SNR. With this goal, it is easy to obtain the power compensation matrix

$$\mathbf{E}_k = \begin{cases} (\mathbf{G}_k^{[k]}\mathbf{F}_k^{[k]})^{-1}(\mathbf{Q}_k)^{\frac{1}{2}} & \text{with power compensation} \\ \mathbf{I}_M & \text{w/o power compensation} \end{cases} . \quad (13)$$

Note that $\mathbf{E}_k$ is a diagonal matrix and the power compensation can be performed with very low complexity. In addition, it is independent of the channel. In such case, the SNR in each subcarrier will be equal and $SNR_k(m) = \rho_{sym}^2\rho_{CH,k}^2/\rho_k^2/\sigma^2$. Note that both transmitter and receiver filter response should be priori known at the transmitter to implement the precoding.

Note that the power compensation algorithm operates on the subband/user level to pre-compensate the selectivity among subcarriers due to the subband filtering operation, in order to ensure that all of the subcarriers are allocated the same power as in the case without subband filtering. In other words, the same as the typical adaptive modulation and coding (ACM) schemes, it is user-specific. Thus, the algorithm will not be affected by the ACM schemes.

D. Desired signal and ICI

For moderate channel conditions and moderate subband bandwidth, it has been claimed in literature that one-tap channel equalization is applicable with negligible interference, even if equation (12) is not satisfied. However, most of the results are based on the qualitative analysis or simulation results. Next, we will analyze the performance loss of the system when orthogonality conditions in equation (12) are not met. The ISI, ICI and ACI will be derived to provide meaningful design guidelines for F-OFDM systems.

Note that in the original F-OFDM system, CP addition copies L_{CP} (normally much smaller than L_O) data samples from the end to the front of the symbol, which is not sufficient to achieve interference-free one-tap equalization. In order to derive the ICI caused by the one-tap channel equalization, let us define a full-size CP adding matrix $\mathbf{R}_O = [\mathbf{0}_{L_O\times(N-L_O)}, \mathbf{I}_{L_O}; \mathbf{I}_N]$, and the difference between two the CP adding matrices $\mathbf{R}_C = \mathbf{R}_O - [\mathbf{0}_{(L_O-L_{CP})\times N}; \mathbf{R}]$ and $\mathbf{R}_C$. In addition, let us define $\mathbf{T}_O = [\mathbf{0}_{N\times L_O}, \mathbf{I}_N]$ as a CP removal matrix of moving the first L_O elements/rows of a vector/matrix. Then we have the following Proposition:

Proposition 2: *Consider the same F-OFDM system defined in Proposition 1 with CP length being L_{CP}. The desired signal and the ICI can be written as:*

$$\mathbf{y}_{DES,k} = \frac{1}{\rho_k}\bar{\mathbf{G}}_k^{[k]}\bar{\mathbf{H}}_k^{[k]}\bar{\mathbf{F}}_k^{[k]}\mathbf{E}_k\mathbf{s}_k + \mathbf{y}_{ICI,k} \quad (14)$$

and

$$\mathbf{y}_{ICI,k} = -\frac{1}{\rho_k}\mathbf{D}_k^H\mathbf{T}_O\mathbf{C}_k\mathbf{B}_k\mathbf{A}_k\mathbf{R}_C\mathbf{D}_k\mathbf{E}_k\mathbf{s}_k . \quad (15)$$

The average power of ICI at the m-th subcarrier of k-th subband $P_{ICI,k}(m) = \mathcal{E}|y_{ICI,k}(m)|^2$ can be expressed as:

$$P_{ICI,k}(m) = \frac{\rho_{sym}^2\rho_{CH,k}^2}{\rho_k^2}\sum_{i=0}^{M-1}\gamma_k(m,i,0,0) , \quad (16)$$

where $\gamma_k(m,i,0,0)$ is defined in equation (17). When $L_{CP} \geq L_O$, we have $\mathbf{R}_C = \mathbf{0}$, resulting in $\mathbf{y}_{ICI,k} = \mathbf{0}$ and $P_{ICI,k}(m) = 0$.

Proof: See Appendix B. ∎

Equation (14) implies that to enable one-tap channel equalization, the ICI will exist in the system. The level of the interference depends on the filter and CP length. Note that due to the filter ramping-up and ramping-down, the product $\mathbf{A}_k\mathbf{R}_C$ could be considerately small when the filter has good time localization (i.e., the filter energy is mostly concentrated in the middle of the filter taps). This will also be shown in the simulation results to illustrate the negligible interference in considered cases.

E. ISI Analysis

Proposition 3: *Considering the same F-OFDM system defined in Proposition 1, the power of ISI defined in (7) can be written as*:

$$P_{ISI,k}(m) = \frac{\rho_{sym}^2\rho_{CH,k}^2}{\rho_k^2}\sum_{\substack{e=-1,\\ e\neq 0}}^{1}\sum_{\substack{d=-1,\\ d\neq 0}}^{1}\sum_{n=0}^{N-1}\gamma_k(m,n,e,d) . \quad (19)$$

The proof can be done following the steps similar to the ICI derivations in (16) and to save space, it is omitted in this paper.

Proposition 3 implies that the level of ISI is dependent on the filter design, subband bandwidth and CP length. Quantitatively, according to the ISI expression in equation (19), the filtered signal tail (and head) might overlap with the current symbol creating ISI and the value could be significantly small when the CP length is sufficiently large and/or the filter is well localized in time domain[5]. This may restrict the applicable scenarios of F-OFDM system. However, with the analytical derivation in equation (19), we can always calculate the ISI level to guide the system design.

F. ACI Analysis

Proposition 4: *Consider the same F-OFDM system defined in Proposition 1. The time differences between the k-th and i-th subband is $\tau_k(i)$ (i.e., synchronization error between the subbands), i.e., the first sample of the i-th subband is delayed $\tau_k(i)$, compared to the first sample of the k-th subband. The*

[5]The filter shape decides how dense does the energy distribute and the CP length decide how long does the interference overlap to the interested symbol. One should note that interference energy distribution is monotonously decreased from the head of the symbol to the middle, i,e., most of the interference energy could be reserved in the CP zone [7].

$$\gamma_i(q,n,e,d) = \sum_{l_1=0}^{L_{SYM}-1} \sum_{l_2=0}^{l_1} \sum_{r=l_1-l_2}^{L_{SYM}-1} \beta_i(n,e,l_1,l_2)\eta_i(q,r,r-l_1+l_2)R_i(r-l_1-dL_{SYM}+\tau_k(i)+\mu_3 L_s)$$
$$+ \sum_{l_1=0}^{L_{SYM}-1} \sum_{l_2=l_1}^{L_{SYM}-1} \sum_{r=l_1-l_2}^{L_{SYM}-1-(l_2-l_1)} \beta_i(n,e,l_1,l_2)\eta_i(q,r,r-l_1+l_2)R_i(r-l_1-dL_{SYM}+\tau_k(i)+\mu_3 L_s) \ ,$$

$$\text{where} \quad \alpha_i(n,e,l) = Q_i(n,n) \sum_{m=0}^{\mu_1-1} e^{j\cdot\frac{2\pi(m-\mu_2)[(i-1)M+n]}{N}} a_i(l-m-eL_{SYM}) \ , \tag{17}$$

$$\beta_i(n,e,l_1,l_2) = \alpha_i(n,e,l_1)\alpha_i(n,e,l_2)^* \ ,$$

$$\theta_i(q,r) = \sum_{p=0}^{N-1} e^{-j\cdot 2\pi p[(i-1)M+q-1]/N} c_i(p-r+\mu_3(L_F-L_s-1)+\mu_2) \ ,$$

$$\eta_i(q,r_1,r_2) = \theta_i(q,r_1)\theta_i(q,r_2)^* \ ,$$

$$\text{where } \mu_1 = L_{SYM},\ \mu_2 = L_{CP} \text{ and } \mu_3 = 1 \text{ for ACI and ISI. ,}$$
$$\mu_1 = L_O - L_{CP},\ \mu_2 = L_O \text{ and } \mu_3 = 0 \text{ for ICI.} \tag{18}$$

power of ACI of the m-th subcarrier in the k-th subband can be written as

$$P_{ACI,k}(m) = \sum_{\substack{i=1,\\ i\neq k}}^{K} \frac{\rho_{sym}^2 \rho_{CH,i}^2}{\rho_i^2} \sum_{e=-1}^{1} \sum_{d=-1}^{1} \sum_{n=0}^{N-1} \gamma_i(m,n,e,d) \ . \tag{20}$$

Again, the proof can be done by following the steps similar to ICI derivations and to save space, it is omitted here.

Equation (20) gives an analytical result of how much ACI an asynchronous system generate and provides a guideline for the system and filter design. It is a general case and can be boiled down to the the OFDM system when the filter length is set to 1. However, in this case, the system might suffer from much larger ACI due to the lack of subband filtering protection.

G. One-tap channel equalization for asynchronous F-OFDM

Based on the derived signal model in the presence of insufficient CP length for non-synchronized F-OFDM system, the channel equalization algorithms can be updated accordingly. In this paper, we consider ZF and MMSE based linear equalization algorithms. The equalizer for the m-th subcarrier can be expressed as

$$W_k(m) = \frac{\phi^H}{|\phi|^2 + \nu[\sigma_e(m)]^2/\rho_{sym}^2} \ , \tag{21}$$

where $\phi = \bar{G}_k^{[k]}(m)\bar{H}_k^{[k]}(m)\bar{F}_k^{[k]}(m)E_k(m)$. $\nu = 0$ and $\nu = 1$ correspond to ZF and MMSE equalizer, respectively. $[\sigma_e(m)]^2 = P_{ICI,k}(m) + P_{ACI,k}(m) + P_{ISI,k}(m) + \sigma^2 Q_k(m,m)$ is the effective interference-plus-noise power for the m-th subcarrier of the k-th subband taking ISI, ICI and ACI and power compensation into consideration.

IV. Multi-rate F-OFDM System and ISubBI Cancelation

The SR implementation of the F-OFDM system has been presented in Section II with comprehensive performance analysis in Section III. However, the SR implementation may suffer from 2-3 orders higher computational complexity. For instance, consider a system with $K = 100$ subbands, each subband contains $M = 12$ subcarriers and the filter length is $L_F = N/2 = 600$. Assuming downlink transmission, the overall complexity at the base station could be 100 times higher than an OFDM system. On the other hand, at the user device side, the high sampling-rate baseband filtering and FFT operation (e.g., 2048-point FFT) is not necessary, especially for narrow band low cost low complexity IoT devices. Next, we will propose a low complexity MR implementation for F-OFDM system. However, unlike SR method, MR system generates residual image signals (i.e., ISubBI) causing performance loss due to the sampling rate mismatch. In order to mitigate the ISubBI, we propose a low complexity ISubBI cancelation algorithm to improve the performance of the proposed MR implementation.

A. Multi-rate F-OFDM system

The proposed MR F-OFDM system for downlink transmission is shown in Fig. 1. Unlike SR system which uses corresponding columns of an N-point IDFT/DFT processing to map the signal to a subband, MR system uses low-dimension full size IDFT (IDFT size is the same as the number of subcarriers in one subband, e.g., $M = 12$) that spreads the signal across the *whole* baseband bandwidth. The following up-sampling operation squeezes the signal into $1/K$ of the full bandwidth. According to the sampling theorem, it creates $(K-1)$ image signals in adjacent bands and an anti-image subband filter is required to eliminate the image signals. Nevertheless, the residual image signal will create the ISubBI in the system due to non-ideal filters, which may degrade system performance in comparison with the SR system [27]. Besides complexity reduction due to low dimension DFT, data sparsity implies that the filtering operation could also significantly reduce the system complexity by taking advantage of the up-sampling operation, particularly, when the filter length is long (and it is critical to reduce the OoBE and interference level).

To reduce the PAPR, DFT spreading can be adopted in the uplink transmission. With MR implementation, a system with

the DFT and IDFT processing will be equivalent to a filtered single carrier system.

B. MR Signal Model and ISubBI

For an insightful analysis and to focus on ISubBI, we will omit ISI, ICI and ACI in the derivations based on the following reasons: 1), the MR system may generate significantly higher interference (i.e., ISubBI) than ISI, ICI and ACI; 2), the MR implementation will not change ISI, ICI and ACI power significantly and the derivations for MR system are trivial; 3), ZF based ISubBI cancelation algorithm is preferred since it does not require interference and noise power, and therefore, it is not related to ISI, ICI and ACI.

With up- and down-sampling, the received signal of the k-th subband can be written as

$$\begin{aligned}\mathbf{y}_k^{MR} &= \sum_{l=1}^{K}\frac{1}{\rho_l}\mathbf{V}^H\mathbf{U}^H\mathbf{T}\mathbf{C}_k\mathbf{B}_l\mathbf{A}_l\mathbf{R}\mathbf{U}\mathbf{V}\mathbf{E}_l\mathbf{s}_l+\tilde{\mathbf{v}}_k\\ &= \sum_{l=1}^{K}\sum_{m=1}^{K}\bar{\mathbf{G}}_k^{[m]}\bar{\mathbf{H}}_k^{[m]}\bar{\mathbf{F}}_l^{[m]}\mathbf{E}_l\mathbf{s}_l+\tilde{\mathbf{v}}_k\ , \end{aligned}\tag{22}$$

where $\mathbf{V}$ is normalized M-point IDFT matrix and $\mathbf{U}$ is the up-sampling matrix by a factor of K. Note that in equation (22), we have used $\mathbf{D}^H\mathbf{U}\mathbf{V}=[\mathbf{I}_M,\mathbf{I}_M,\cdots,\mathbf{I}_M]\in\mathbb{R}^{M\times N}$.

Thus, the desired signal and the interference can be written as

$$\mathbf{y}_{DES,k}^{MR}=\sum_{m=1}^{K}\bar{\mathbf{G}}_k^{[m]}\bar{\mathbf{H}}_k^{[m]}\bar{\mathbf{F}}_k^{[m]}\mathbf{E}_k\mathbf{s}_k\tag{23}$$

and the ISubBI can be expressed as

$$\mathbf{y}_{ISubBI,k}^{MR}=\sum_{l=1,l\neq k}^{K}\sum_{m=1}^{K}\bar{\mathbf{G}}_k^{[m]}\bar{\mathbf{H}}_k^{[m]}\bar{\mathbf{F}}_l^{[m]}\mathbf{E}_l\mathbf{s}_l\ .\tag{24}$$

Comparing to the desired signal expressed in (11), it can be seen that the signal expression in equation (23) is a summation of K terms, which is due to the image signals generated in the up- and down-sampling in MR processing. Specifically, up- and down-sampling by a factor of K results in $K-1$ image signals in adjacent spectrum except the original one, and those signals will destroy the circular convolution property and one-tap channel/filter equalization will cause interference.

For the ISubBI in (24), it is essentially ACI since the interference is caused by the adjacent subbands. Instead of one ACI signal per adjacent subband in SR system, K ACI signals in each subband are generated in MR system, resulting in two layers of summations as shown in (24).

Note that with the subband filtering, the IsubBI can be mitigated significantly when the subband is far away from the current subband. However, According to the FFR in Fig. 2, the edge subcarriers in the adjacent (stopband) subband can still generate considerately large interference. Next, we will propose low-complexity algorithms to enable one-tap equalization to detect $\mathbf{s}_k$.

C. ISubBI Cancelation

According to our analysis and filter frequency response Fig. 2, the matrix element of $\bar{\mathbf{G}}_k^{[m]}$ and $\bar{\mathbf{F}}_k^{[m]}$ are non-trivial only if $|m-k|\leq 1$. In other words, only adjacent subbands generate non-trivial interference. Thus, we have the approximated desired signal and interference as

$$\begin{aligned}\tilde{\mathbf{y}}_{DES,k}^{MR} &= (\bar{\mathbf{G}}_k^{[k-1]}\bar{\mathbf{H}}_k^{[k-1]}\bar{\mathbf{F}}_k^{[k-1]}+\bar{\mathbf{G}}_k^{[k]}\bar{\mathbf{H}}_k^{[k]}\bar{\mathbf{F}}_k^{[k]}\\ &+ \bar{\mathbf{G}}_k^{[k+1]}\bar{\mathbf{H}}_k^{[k+1]}\bar{\mathbf{F}}_k^{[k+1]})\mathbf{E}_k\mathbf{s}_k\end{aligned}\tag{25}$$

and

$$\begin{aligned}\tilde{\mathbf{y}}_{ISubBI,k}^{MR}=&\bar{\mathbf{G}}_k^{[k-1]}\bar{\mathbf{H}}_k^{[k-1]}\bar{\mathbf{F}}_{k-1}^{[k-1]}\mathbf{E}_{k-1}\mathbf{s}_{k-1}\\ &+\bar{\mathbf{G}}_k^{[k]}\bar{\mathbf{H}}_k^{[k]}\bar{\mathbf{F}}_{k-1}^{[k]}\mathbf{E}_{k-1}\mathbf{s}_{k-1}\\ &+\bar{\mathbf{G}}_k^{[k]}\bar{\mathbf{H}}_k^{[k]}\bar{\mathbf{F}}_{k+1}^{[k]}\mathbf{E}_{k+1}\mathbf{s}_{k+1}+\bar{\mathbf{G}}_{k+1}^{[k]}\bar{\mathbf{H}}_k^{[k+1]}\bar{\mathbf{F}}_{k+1}^{[k+1]}\mathbf{E}_{k+1}\mathbf{s}_{k+1}\end{aligned}\tag{26}$$

By noting that $\bar{\mathbf{G}}_l^{[m]}=\bar{\mathbf{G}}_{l+i}^{[m+i]}$ and $\bar{\mathbf{F}}_l^{[m]}=\bar{\mathbf{F}}_{l+i}^{[m+i]}$ and defining

$$\begin{aligned}\mathbf{Z}_0 &= \bar{\mathbf{G}}_k^{[k-1]}\bar{\mathbf{H}}_k^{[k-1]}\bar{\mathbf{F}}_k^{[k-1]}\\ &+\bar{\mathbf{G}}_k^{[k]}\bar{\mathbf{H}}_k^{[k]}\bar{\mathbf{F}}_k^{[k]}+\bar{\mathbf{G}}_k^{[k+1]}\bar{\mathbf{H}}_k^{[k+1]}\bar{\mathbf{F}}_k^{[k+1]}\end{aligned}\tag{27}$$

$$\mathbf{Z}_1=\bar{\mathbf{G}}_k^{[k-1]}\bar{\mathbf{H}}_k^{[k-1]}\bar{\mathbf{F}}_{k-1}^{[k-1]}+\bar{\mathbf{G}}_k^{[k]}\bar{\mathbf{H}}_k^{[k]}\bar{\mathbf{F}}_{k-1}^{[k]}\tag{28}$$

$$\mathbf{Z}_2=\bar{\mathbf{G}}_k^{[k]}\bar{\mathbf{H}}_k^{[k]}\bar{\mathbf{F}}_{k+1}^{[k]}+\bar{\mathbf{G}}_{k+1}^{[k]}\bar{\mathbf{H}}_k^{[k+1]}\bar{\mathbf{F}}_{k+1}^{[k+1]}\ .\tag{29}$$

Consider the entire bandwidth signal, the signal model for the MR F-OFDM system can be expressed as:

$$\mathbf{y}^{MR}=\mathbf{X}\mathbf{E}\mathbf{s}+\tilde{\mathbf{v}}\ ,\tag{30}$$

where $\mathbf{E}=\text{diag}[\mathbf{E}_1;\cdots;\mathbf{E}_K]$ and $\tilde{\mathbf{v}}=[\tilde{\mathbf{v}}_1;\cdots;\tilde{\mathbf{v}}_K]$ are the power compensation matrix and noise for the whole bandwidth. The mixture matrix

$$\mathbf{X}=\begin{pmatrix}\mathbf{Z}_0 & \mathbf{Z}_2 & \mathbf{0} & \mathbf{0} & \mathbf{0} & \cdots & \psi\mathbf{Z}_1\\ \mathbf{Z}_1 & \mathbf{Z}_0 & \mathbf{Z}_2 & \mathbf{0} & \mathbf{0} & \cdots & \mathbf{0}\\ \mathbf{0} & \mathbf{Z}_1 & \mathbf{Z}_0 & \mathbf{Z}_2 & \mathbf{0} & \cdots & \mathbf{0}\\ \vdots & \ddots & \ddots & \ddots & \ddots & \cdots & \mathbf{0}\\ \vdots & \vdots & \ddots & \ddots & \ddots & \ddots & \mathbf{0}\\ \mathbf{0} & \cdots & \mathbf{0} & \mathbf{0} & \mathbf{Z}_1 & \mathbf{Z}_0 & \mathbf{Z}_2\\ \psi\mathbf{Z}_2 & \cdots & \mathbf{0} & \mathbf{0} & \mathbf{0} & \mathbf{Z}_1 & \mathbf{Z}_0\end{pmatrix},\tag{31}$$

where $\psi=1$ if all of the subband are occupied, i.e., the last subband will generate (receive) interference to (from) the first one; and $\psi=0$ if guard band is applied to the system, i.e., the first and the last subbands will not interfere each other due to the guardband protection.

Apparently, the desired signals in any subband is interfered by the adjacent subbands. To eliminate the interference, we can process the original transmitted signal $\mathbf{s}$ at the transmitter side, or jointly process the received signal at the receiver side. Note that in order to take the advantage of the base station's computational capability, it is preferred to perform interference elimination at the base station no matter for uplink or downlink transmission. In other words, for downlink transmission, we precode the transmitted signal $\mathbf{s}$ at the transmitter and for uplink transmission, we can perform joint detection on the received signal $\mathbf{y}^{MR}$. However, in this paper, we will consider the downlink transmission as an example.

1) Channel-dependent ISubBI Cancelation Algorithm: Let us first consider the downlink case with the precoding matrix $\mathbf{P}$ used to pre-cancel the interference as follows:

$$\mathbf{y}^{MR} = \mathbf{XPEs} + \tilde{\mathbf{v}} \ . \tag{32}$$

We can use the standard ZF method to get the optimal $\mathbf{P}$ as

$$\mathbf{P} = \frac{1}{\rho_P}\mathbf{X}^{-1} \ , \tag{33}$$

where $\frac{1}{\rho_P}$ is the normalization factor and $\rho_P = \sqrt{\text{trace}[\mathbf{X}^{-1}(\mathbf{X}^{-1})^H]/N}$.

Calculation of $\mathbf{P}$ requires a matrix inversion operation, which could be very complex when N is large, though the matrix $\mathbf{X}$ is well structured with only some main diagonal elements being non-zero. In addition, we have to update $\mathbf{P}$ in channel coherence time since $\mathbf{X}$ is a function of the channel, leading to high system computational complexity. In addition, this algorithm requires the knowledge of channel state information at the transmitter, which might be unavailable or inaccurate in some communication scenarios. Next, we will introduce new algorithms that do not rely on the channel state information and the precoding matrix/detection matrix can be calculated offline.

2) Channel-independent ISubBI Cancelation Algorithm: Assuming that the channel frequency response is flat across the three considered subbands, we can approximate $\mathbf{Z}_0$, $\mathbf{Z}_1$ and $\mathbf{Z}_2$ as follows:

$$\tilde{\mathbf{Z}}_0 = \bar{\mathbf{H}}_k^{[k]}\hat{\mathbf{Z}}_0 \ , \tag{34}$$

$$\tilde{\mathbf{Z}}_1 = \bar{\mathbf{H}}_k^{[k]}\hat{\mathbf{Z}}_1 \ , \tag{35}$$

$$\tilde{\mathbf{Z}}_2 = \bar{\mathbf{H}}_k^{[k]}\hat{\mathbf{Z}}_2 \tag{36}$$

and $\hat{\mathbf{Z}}_0 = \bar{\mathbf{G}}_k^{[k-1]}\bar{\mathbf{F}}_k^{[k-1]} + \bar{\mathbf{G}}_k^{[k]}\bar{\mathbf{F}}_k^{[k]} + \bar{\mathbf{G}}_k^{[k+1]}\bar{\mathbf{F}}_k^{[k+1]}$, $\hat{\mathbf{Z}}_1 = \bar{\mathbf{G}}_k^{[k-1]}\bar{\mathbf{F}}_{k-1}^{[k-1]} + \bar{\mathbf{G}}_k^{[k]}\bar{\mathbf{F}}_{k-1}^{[k]}$ and $\hat{\mathbf{Z}}_2 = \bar{\mathbf{G}}_k^{[k]}\bar{\mathbf{H}}_k\bar{\mathbf{F}}_{k+1}^{[k]} + \bar{\mathbf{G}}_{k+1}^{[k]}\bar{\mathbf{F}}_{k+1}^{[k+1]}$

Then we can rewrite (32) as

$$\mathbf{y}^{MR} \approx \tilde{\mathbf{H}}_k\tilde{\mathbf{X}}\mathbf{Es} + \tilde{\mathbf{v}} \ , \tag{37}$$

where $\tilde{\mathbf{X}}$ has the same structure as $\mathbf{X}$, only replacing $\mathbf{Z}_0$, $\mathbf{Z}_1$ and $\mathbf{Z}_2$ by $\hat{\mathbf{Z}}_0$, $\hat{\mathbf{Z}}_1$ and $\hat{\mathbf{Z}}_2$, respectively. Note that different from $\mathbf{T}$, $\tilde{\mathbf{T}}$ is unrelated to the channel coefficients. $\tilde{\mathbf{H}}_k = \text{diag}\{\mathbf{h}_k\}$ is the diagonal channel matrix for all subcarriers.

Equation (37) decouples the channel from the filter response and shows point-wise multiplication of the signal and channel. This is critical for the one-tap channel equalization and calculating the channel-independent ISubBI precancelation matrix. For the downlink transmission, we can perform precoding based on the channel-independent matrix as

$$\mathbf{P}_2 = \frac{1}{\tilde{\rho}_P}\tilde{\mathbf{X}}^{-1} \ , \tag{38}$$

where $\frac{1}{\tilde{\rho}_P}$ is the normalization factor and $\rho_P = \sqrt{\text{trace}[\tilde{\mathbf{X}}^{-1}(\tilde{\mathbf{X}}^{-1})^H]/N}$. Note that at the receiver, one-tap channel equalization should be performed since the precoding process does not consider the channel coefficient.

3) Partly Subband Bandwidth ISubBI Cancelation Algorithm: The interference mixture submatrices $\mathbf{Z}_1$ and $\mathbf{Z}_2$ are diagonal matrices and according to the analysis in Section III and FFR in Fig. 2, the elements at the edges of $\mathbf{Z}_1$ and $\mathbf{Z}_2$ have significantly higher values than in the middle of the matrices. For example, $|Z_1(1)| = |Z_1(M)| > |Z_1(2)| = |\ Z_1(M-1)| > |Z_1(M)| > |Z_1(3)| = |Z_1(M-2)| > \cdots > Z_1(M/2)$. Therefore, the ISubBI at the edge of each subband is much stronger than in the middle of the subband. This inspires us to only consider the edge subcarriers of each subband instead of canceling the ISubBI over the whole bandwidth to further reduce the complexity.

Let us assume the L edge subcarriers (on both left and right sides, e.g., when $L = 2$, the first two subcarriers from the left, and the last two from the right) of each subband generate serious interference. We can select the edge subcarriers and build a small dimension signal model as

$$\mathbf{y}_L^{MR} = \mathbf{X}_L\mathbf{P}_L\mathbf{E}_L\mathbf{s}_L + \mathbf{v}_L \ , \tag{39}$$

where $\mathbf{s}_L$ is defined as $\mathbf{s}_L = [\hat{\mathbf{s}}_1; \cdots; \hat{\mathbf{s}}_K]$ and $\hat{\mathbf{s}}_k = [s_k(1), s_k(2), \cdots, s_k(L), s_k(M-L+1), s_k(M-L+2), \cdots, s_k(M)]^T$. $\mathbf{y}_L^{MR}$ and $\mathbf{v}_L$ are the received signal and noise vector at the selected subcarriers over the whole bandwidth, respectively. $\mathbf{X}_L$ has the same structure as $\mathbf{X}$ but $\mathbf{Z}_0$, $\mathbf{Z}_1$ and $\mathbf{Z}_2$ are replaced by $\mathbf{Z}_{L,0}$, $\mathbf{Z}_{L,1}$ and $\mathbf{Z}_{L,2}$, i.e. $2L \times 2L$ diagonal matrices taking the first and last diagonal elements of $\mathbf{Z}_0$, $\mathbf{Z}_1$ and $\mathbf{Z}_2$, respectively. Similarly, $\mathbf{E}_L$ is a matrix that takes the corresponding elements of $\mathbf{E}$. Then the proposed ISubBI cancelation algorithms in (33) and (38) can be updated as follows:

$$\mathbf{P}_L = \frac{1}{\rho_{P,L}}{\mathbf{X_L}}^{-1} \tag{40}$$

and

$$\tilde{\mathbf{P}}_L = \frac{1}{\tilde{\rho}_{P,L}}\tilde{\mathbf{X}}_{\mathbf{L}}^{-1} \ , \tag{41}$$

where $\frac{1}{\rho_{P,L}}$ and $\frac{1}{\tilde{\rho}_{P,L}}$ are the power normalization factors.

Note that (40) and (41) are general cases of (33) and (38), respectively. When $L = M$, (40) and (41) will boil down to (33) and (38).

D. Computational complexity

1) Computational Complexity of ISubBI Cancelation: Note that the computational complexity of the ISubBI cancelation algorithm involves complexity of precoding matrix (e.g., $\tilde{\mathbf{P}}_L$) calculation and it depends on the dimension of interference matrix (e.g., $\tilde{\mathbf{X}}_L$). Let us first consider the channel-independent case with the number of cancelation subcarriers being L. Note that $\tilde{\mathbf{X}}_L^{-1}$ could be calculated in advance for $\tilde{\mathbf{P}}_L$. Then $\tilde{\mathbf{P}}_L\mathbf{s}_L$ needs $6LK$ complex multiplications. Note that generally taking $L = 1$ or 2 is sufficient and the complexity could be significantly lower than the FFT operation in OFDM system, as shown in Fig. 3.

For the channel-dependent case, it relies on how fast the channel changes and how often the precoder updates. Let us consider the worst-case that $\mathbf{X}_L$ changes in every F-OFDM symbol, then the total complexity will be $\mathcal{O}((2LK)^3) + 6LK$

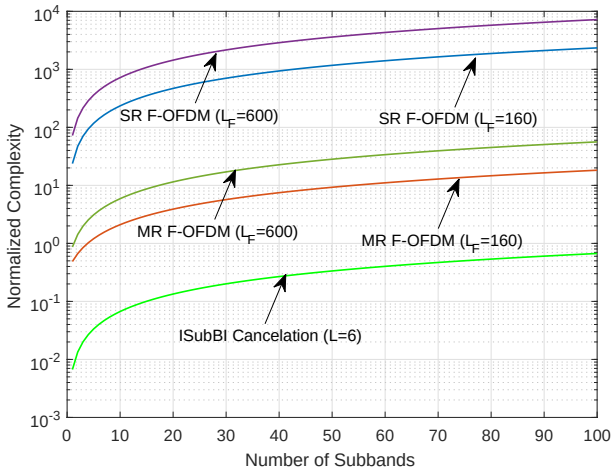

Fig. 3. SR and MR F-OFDM system complexity with $M = 12$ (Normalized by OFDM system).

complex multiplications with $\mathcal{O}((2LK)^3)$ being the complex of matrix $\mathbf{X}_L$ inversion calculation.

2) Computational Complexity SR and MR implementations: Note that the overall complexity at the transmitter and receiver are similar and here we only consider the transmitter complexity for the downlink transmission. For the SR implementation with K subbands, K IFFT operations are required each requiring $(N\log_2(N) - 3N + 4)/2$ complex multiplications [20]. The filtering operation needs $L_F N$ complex multiplications. Therefore, in total, $(N\log_2(N)-3N+4)/2+L_F N$ complex multiplications are performed per subband and $K((N\log_2(N)-3N+4)/2+L_F N)$ complex multiplications are performed for the whole bandwidth.

For the MR implementation, each subband requires $(N\log_2(N) - 3N + 4)/2$ complex multiplications; for the filtering operation, it needs $L_F M$ complex multiplications. In total, $K((M\log_2(M) - 3M + 4)/2 + L_F M)$ complex multiplications are needed for the whole bandwidth. Note that MR subband filtering takes the advantage of up-sampling operation for computational complexity since the data after up-sampling is sparse.

The transmitter computational complexity in terms of the multiplication of the SR and MR systems for both implementations is shown in Figure 3. Note that the complexity is normalized by the OFDM system (i.e., $(N\log_2(N)-3N+4)/2$). We can see that SR implementation complexity is significantly higher than OFDM system (up to 1000 times when number of subbands is 100, which roughly corresponds to 20MHz bandwidth in LTE), while the MR system can achieve comparable complexity as the OFDM system. In addition, the ISubBI cancelation algorithm for the MR implementation is negligible with $L = 6$.

V. Numerical results

In this section, we use Monte-Carlo simulations to verify the accuracy of derived F-OFDM system signal models and the derived interference power in (16), (19) and (20) proposed in Propositions 2, 3 and 4. In addition, the proposed power compensation algorithm and ISubBI cancelation algorithms for MR F-OFDM will be examined.

Unless otherwise specified, the following common parameters are used for simulations: the signal is modulated using 16-QAM (Quadrature amplitude modulation) with power normalized to unity and the input SNR is controlled by the noise variance. We use the root-raised-cosine (RRC) Windowed Sinc filter at transmitter and matched filter at receiver for all simulations [7], [18]. The filter length and CP length are 50% and 7% of a symbol duration, respectively [7], [18]. Each subband contains 12 subcarriers and in total 100 subbands are used. For the ACI parameter τ_i, we assume it has uniform random distribution between $[0, N]$. The LTE Extended Pedestrian-A (EPA) channel [4] is assumed in all simulations. We also provide the results for OFDM systems as benchmark for comparison.

A. OoBE and PAPR

F-OFDM performance in terms of OoBE and PAPR is examined in Fig. 4 for CP-OFDM, original SR F-OFDM, proposed MR F-OFDM and MR F-OFDM with ISubBI cancelation. Note that 3 subbands are considered for OoBE. It can be seen that the F-OFDM system can achieve significantly lower OoBE than the OFDM system for both SR or MR systems. However, the MR system performs slightly worse than the SR system due to the (residual) image signals. In addition, the MR system with ISubBI cancelation does not cause significant increase in OoBE. Comparing the F-OFDM with and without power compensation, we can see that the power is evenly distributed in the passband of F-OFDM with power compensation; while the filter response selectivity shows in the one without power compensation.

In terms of PAPR, SR F-OFDM system performs similar to the CP-OFDM system. However, ISBI cancelation algorithm does not bring noticeable PAPR ($\approx$ 0.01 dB) increase, no matter for SR or MR systems. In addition, compared to SR F-OFDM, MR F-OFDM increases PAPR by around 0.7 dB. The reason is that the upsampling process in the MR implementation will make the power distribution among symbols wider than the SR case. That may degrade the efficiency of the power amplifier in the transmitter. Some PAPR reduction algorithms such as DFT spreading can be adopt on top of SR/MR F-OFDM.

B. ICI, ISI and ACI

Now we examine the impact of system parameters (e.g., filter length, CP length, etc.) on the system performance and compare our analytical results with the simulation results in terms of the power of the ICI, ISI and ACI in an asynchronous system. To make the comparison clear for this simulation, we consider in total 36 subcarirers are split into 3 subbands each containing 12 subcarriers. In addition, $\tau_1 = \tau_3 = N/4$ and $\tau_2 = 0$. However, a general case will be considered in the next simulations. Fig. 5 shows the analytical and simulated interference power for the second subband (which is in the middle). It can be seen that all of the analytical results

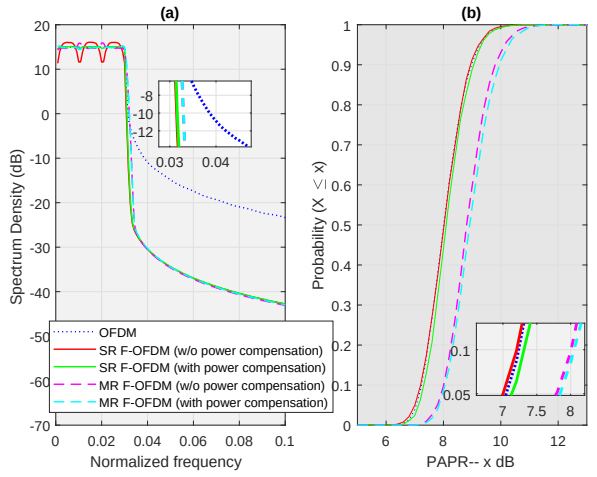

Fig. 4. OoBE and PAPR for OFDM, SR F-OFDM, MR F-OFDM (with and

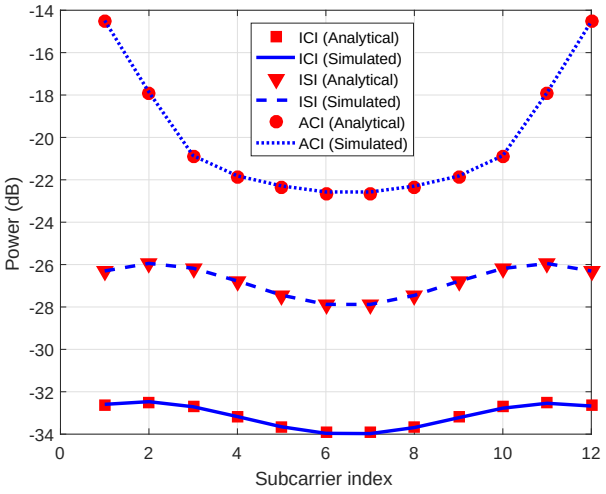

Fig. 5. Analytical and simulated ICI, ISI and ACI power versus subcarrier index.

match the simulation results which shows the effectiveness and accuracy of the derived signal models and interference power in (16), (19) and (20). In addition, due to the asynchronousity among the subbands, the ACI level is significantly higher than ICI and ISI. However, ISI shows larger impact on the system than ICI. Since the analytical and simulated results match very well, in the next, we will only show either analytical or simulated results for clarity.

In order to show the relationship between the filter length and the ACI level, the analytical results for ACI versus subcarrier index with different filter lengths are shown in Fig. 6. It can be seen that the ACI level drops monotonically when the filter length increases, especially in the middle of the subband. The reason is that longer CP results in higher probability of synchronization between subbands. However, in all cases, the F-OFDM system can mitigate the ACI effectively as compared with the OFDM system.

The impact of CP length on the system performance in terms of ICI and ISI at the first subcarrier (the worst-case) in one subband is shown in Fig. 7 (a). It can be seen that both ICI and ISI drop when the CP length increases. However, ICI is more sensitive to the change than ISI and it is negligible compared

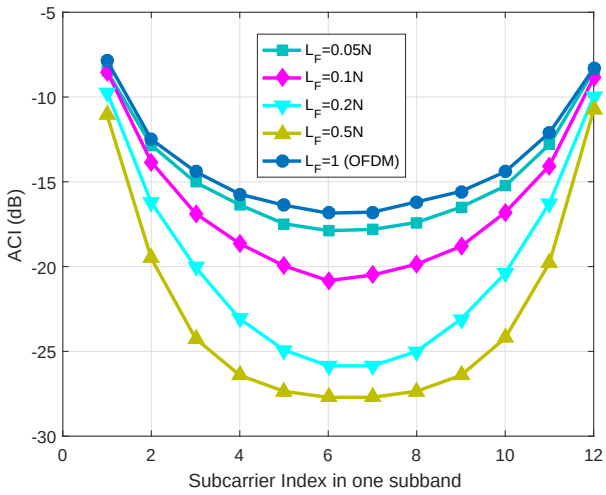

Fig. 6. ACI power versus subcarrier index with different filter length L_F ($L_{CP} = 0.07N$).

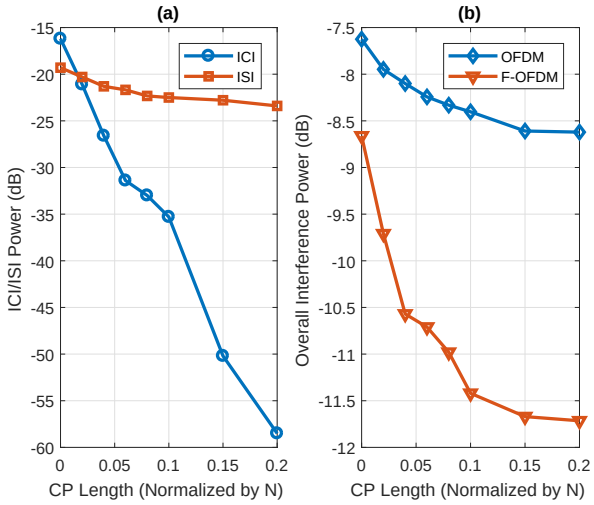

Fig. 7. (a) ICI and ISI power versus CP length L_{CP}, (b) overall interference power versus CP length. ($L_F = N/2$ for F-OFDM).

to ISI when the CP length is set as 7% of the symbol duration. Since ISI does not drop significantly even with large CP length, in such a case, filter optimization should be considered to further reduce the ISI level. One possible solution is to take the system parameter information into consideration to balance ICI, ISI and ACI and to minimize the overall interference [30], [31]. Moreover, the channel statistic information can also be considered to further improve the performance.

Fig. 7 (b) compares the overall interference at the first subcarrier (the worst case) in OFDM and F-OFDM system in asynchronous systems. It can be seen that the F-OFDM suffers from smaller overall interference than the OFDM system, thus, it expects a better BER performance than OFDM system.

C. Bit Error Rate

We first investigate the performance of the SR F-OFDM system with and without power compensation in terms of BER in asynchronous scenarios with OFDM system as a benchmark. Note that different subband bandwidth M and

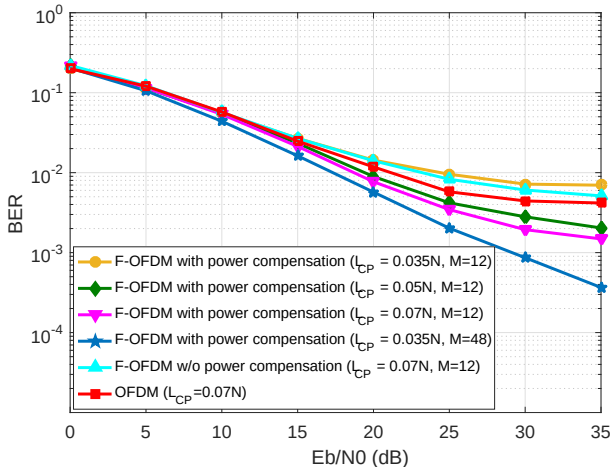

Fig. 8. SR F-OFDM BER performance with different CP length L_{CP} and filter length L_F for asynchronous system.

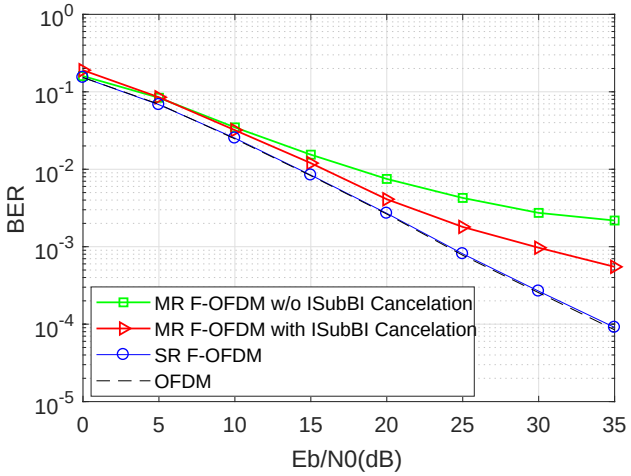

Fig. 9. MR F-OFDM system BER performance for synchronous system

.

CP length L_{CP} are considered in the simulation to show the system's sensitivity to the parameters. It can be seen from Fig. 8 that the performance is better with longer CP length or larger subband bandwidth. The reason is that larger subband bandwidth means that more energy is concentrated in the mainlobe and the leakage to the adjacent symbols is smaller. Therefore, it generates less ISI into the adjacent symbols. The OFDM system shows an obvious error floor in high SNR region due to ACI among the subbands. On the other hand, F-OFDM shows robustness to such kind of interference with moderately large subband bandwidth and CP length.

In addition, it can be seen that the performance difference with and without power compensation at the transmitter is significant, which concludes that the power compensation is necessary at the cost of negligible increase in computation complexity.

Finally, we examine the performance of the proposed MR F-OFDM system in synchronous systems with and without ISubBI cancelation shown in Fig. 9. In this simulation, we use $L_{CP} = 0.07N$ and $M = 12$. We adopt the channel-independent partial subband bandwidth ISubBI cancelation algorithm derived in (41) with $L = 2$. In addition, Quadrature phase-shift keying (QPSK) modulated signal is used to target the low data-rate low complexity mMTC scenarios [9]. All other simulation parameters are specified in the first and second paragraphs of Section V to conserve space. To avoid over-crowded curves associated with multiple parameters (CP length L_{CP}, subband size M and E_b/N_0), we have selected some representatives shown in Fig. 9. It can be seen from the figure that compared with the SR F-OFDM system, the MR F-OFDM has worse BER performance due to the image signals, no matter ISubBI cancelation is applied in the system or not. However, with the ISubBI cancelation, it can achieve a better performance compared to the algorithm without ISubBI cancelation and the gain is significant in high SNR region. In addition, compared to OFDM system, SR F-OFDM shows a slightly degraded performance due to the filter tail overlapping caused ICI/ISI.

VI. Conclusions

The F-OFDM system has been modeled and analyzed in this paper by considering ICI, ISI and ACI for asynchronous scenarios. Several propositions have bee made on the orthogonality conditions of the system and the analytical derivations for ICI, ISI and ACI, which can provide theoretical guidelines for 5G system design. Based on the analytical results, we proposed a power compensation matrix to optimize the subcarrier performance in a subband. In addition, a channel equalization algorithm is proposed by considering the system interference and power compensation. We also proposed a low complexity MR F-OFDM system to support low cost devices. The low complexity MR system comes at the cost of ISubBI and performance loss due to the image signals. A set of ISubBI cancelation algorithms is proposed to mitigate the interference. Simulation results show that our derivations are valid and the proposed MR system can save up to 100 times computational complexity. The proposed ISubBI cancelation algorithm can effectively mitigate the ISubBI with negligible complexity increase.

Acknowledgement

A U.K. patent Multi-Rate Wireless Communication Network (reference number GB1620293.9) related to this work was filed on November 30, 2016. The authors would like to acknowledge the support of the University of Surrey 5GIC (http://www.surrey.ac.uk/5gic) members for this work.

Appendix A
Proof of Proposition 1

Note that the transmitter and receiver filters are convoluted with the channel from the left and right side, respectively. Thus, we can treat the filter (both transmitter and receiver filters) and channel as the effective channel with length $L_{CH}+2L_F-2$. In this case, the F-OFDM system can be treated as a special CP-OFDM system with channel length $L_{CH}+2L_F-2$. We can, therefore, conclude that the system is ISI-free (i.e.,

$\mathbf{y}_{ISI,k} = \mathbf{0}$) when $L_{CP} \geq L_O$. Now let us consider the ICI, which can be rewritten as

$$\mathbf{y}_{DES,k} = \frac{1}{\rho_k}\mathbf{D}_k^H\mathbf{T}\mathbf{C}_k^H\mathbf{B}_k\mathbf{A}_k\mathbf{R}\mathbf{D}_k\mathbf{E}_k\mathbf{s}_k \ . \tag{42}$$

When $L_{CP} \geq L_O$, we have $\mathbf{T}\mathbf{C}^H\mathbf{B}_k\mathbf{A}_k\mathbf{R} = \mathbf{T}\mathbf{C}_k^H\mathbf{R}\mathbf{T}\mathbf{B}_k\mathbf{R}\mathbf{T}\mathbf{A}_k\mathbf{R} = \mathbf{C}_{cir,k}^H\mathbf{B}_{cir,k}\mathbf{A}_{cir,k}$, where $\mathbf{C}_{cir,k}^H$, $\mathbf{B}_{cir,k}$ and $\mathbf{A}_{cir,k}$ are N dimension circular matched filter channel and transmit filter matrices, respectively. Substituting into (42) and write it as

$$\mathbf{y}_{DES,k} = \frac{1}{\rho_k}\mathbf{D}_k^H\ \mathbf{C}_{cir,k}^H\mathbf{D}\mathbf{D}^H\mathbf{B}_{cir,k}\mathbf{D}\mathbf{D}^H\mathbf{A}_{cir,k}\mathbf{D}_k\mathbf{E}_k\mathbf{s}_k \ . \tag{43}$$

By further using the circular convolution property: $\mathbf{D}_k^H\mathbf{C}_k^H\mathbf{D} = [\mathbf{0}_{M\times(k-1)M}, \bar{\mathbf{G}}_k^{[k]}, \mathbf{0}_{M\times(K-k)M}]$, $\mathbf{D}^H\mathbf{A}_k\mathbf{D}_k = [\mathbf{0}_{M\times(k-1)M}, \bar{\mathbf{F}}_k^{[k]}, \mathbf{0}_{M\times(K-k)M}]$ and $\mathbf{D}^H\mathbf{H}_{cir,k}^H\mathbf{D} = \mathrm{diag}(\bar{\mathbf{H}})$, we can obtain $\mathbf{y}_{DES,k} = \frac{1}{\rho_k}\bar{\mathbf{G}}_k^{[k]}\bar{\mathbf{H}}_k\bar{\mathbf{F}}_k^{[k]}\mathbf{E}_k\mathbf{s}_k$.

For the ACI with $0 \leq \tau_i \leq L_{CP} - L_O$, we can follow the same method to write $\mathbf{y}_{ACI,k}$ as:

$$\begin{aligned}\mathbf{y}_{ACI,k} \quad &= \sum_{\substack{i=1,\\ i\neq k}}^{K} \frac{1}{\rho_i}\mathbf{D}_k^H\ \mathbf{C}_{cir,k}^H\mathbf{D}\mathbf{D}^H\mathbf{B}_{cir,k}\mathbf{D}\mathbf{D}^H \\ &\quad \cdot\mathbf{A}_{cir,i}\mathbf{D}_i\mathbf{E}_i\mathbf{s}_i \ .\end{aligned} \tag{44}$$

When $i \neq k$, the non-zero parts of $\mathbf{D}_k^H\mathbf{B}_{cir,k}\mathbf{D}$ and $\mathbf{D}^H\mathbf{A}_{cir,i}\mathbf{D}_i$ do not overlap, leading to $\mathbf{y}_{ACI,k} = \mathbf{0}$.

In summary, we have equation (11) the Proposition 1 when $L_{CP} \geq L_O$ and $0 \leq \tau_i \leq L_{CP} - L_O$.

Appendix B
Proof of Equation (16)

According to the definition of $\mathbf{R}_O$ and $\mathbf{R}_C$, we have $\mathbf{y}_{DES,k} = \frac{1}{\rho_k}\mathbf{D}_k^H\mathbf{T}_O\mathbf{C}_k^H\mathbf{B}_k\mathbf{A}_k\mathbf{R}_O\mathbf{D}_k\mathbf{E}_k\mathbf{s}_k - \frac{1}{\rho_k}\mathbf{D}_k^H\mathbf{T}_O\mathbf{C}_k^H\mathbf{B}_k\mathbf{A}_k\mathbf{R}_C\mathbf{D}_k\mathbf{E}_k\mathbf{s}_k$. According to Proposition 1, we can easily get the first term as $\frac{1}{\rho_k}\bar{\mathbf{G}}_k^{[k]}\bar{\mathbf{H}}_k\bar{\mathbf{F}}_k^{[k]}\mathbf{E}_k\mathbf{s}_k$, then we obtain equations (14) and (15).

To prove (16), we have to write equation (14) as a time series expression:

$$\begin{aligned}y_{ICI,k}(m) \quad &= \sum_{l=0}^{L_{SYM}-1}\sum_{r=0}^{L_{SYM}-1}\sum_{i=0}^{M-1} Q_k(i,i) \\ &\quad \cdot\alpha_m(i,0,l)\theta_i(q,r)b(r-l)s_k(n) \ .\end{aligned} \tag{45}$$

Let us use the fact that $E\{b_k(l_1)b_k^*(l_2)\} = 0$ if $l_1 \neq l_2$ and $E\{b_k(l_1)b_k^*(l_2)\} = R_k(l_1 - l_2)$ if $l_1 = l_2$. Additionally, $E\{s_k(n_1)s_k^*(n_2) = 0\}$ for $n_1 \neq n_2$, therefore, we have equation (16).

References

[1] F. Schaich, B. Sayrac, M. Schubert, H. Lin, K. Pedersen, M. Shaat, G. Wunder, and A. Georgakopoulos, "FANTASTIC-5G: 5G-PPP project on 5G air interface below 6 GHz," in *European Conference on Network and Communications*, 2015.

[2] L. Zhang, A. Ijaz, P. Xiao, and R. Tafazolli, "Multi-service system: An enabler of flexible 5G air interface," *IEEE Communications Magazine*, vol. 55, no. 10, pp. 152–159, OCTOBER 2017.

[3] A. Ijaz, L. Zhang, M. Grau, A. Mohamed, S. Vural, A. U. Quddus, M. A. Imran, C. Foh, and R. Tafazolli, "Enabling Massive IoT in 5G and Beyond Systems: PHY Radio Frame Design Considerations," *IEEE Access*, vol. 4, pp. 3322–3339, 2016.

[4] E. Dahlman, S. Parkvall, and J. Skold, *4G: LTE/LTE-Advanced for Mobile Broadband*. Academic Press, 2011.

[5] L. Zhang, A. Ijaz, P. Xiao, and R. Tafazolli, "Subband filtered multi-carrier systems for multi-service wireless communications," *IEEE Transactions on Wireless Communications*, vol. 16, no. 3, pp. 1893–1907, March 2017.

[6] 5GNOW, "D3.2: 5G waveform candidate selection," Tech. Rep., 2014.

[7] X. Zhang, M. Jia, L. Chen, J. Ma, and J. Qiu, "Filtered-OFDM - enabler for flexible waveform in the 5th generation cellular networks," in *2015 IEEE Global Communications Conference*, Dec 2015, pp. 1–6.

[8] F. Schaich and T. Wild, "Relaxed synchronization support of universal filtered multi-carrier including autonomous timing advance," in *International Symposium on Wireless Communications Systems (ISWCS)*, 2014, pp. 203–208.

[9] L. Zhang, A. Ijaz, P. Xiao, and R. Tafazolli, "Channel equalization and interference analysis for uplink narrowband internet of things (NB-IoT)," *IEEE Communications Letters*, vol. PP, no. 99, pp. 1–1, 2017.

[10] Y. Wang *et al.*, "A Primer on 3GPP Narrowband Internet of Things (NB-IoT)," *[Online]. Available: http://arxiv.org/ftp/arxiv/papers/1606/1606.04171.pdf.*, 2016.

[11] L. Zhang, P. Xiao, A. Zafar, A. ul Quddus, and R. Tafazolli, "FBMC system: An insight into doubly dispersive channel impact," *IEEE Transactions on Vehicular Technology*, vol. PP, no. 99, pp. 1–14, 2016.

[12] B. Farhang-Boroujeny, "OFDM versus filter bank multicarrier," *IEEE Signal Processing Magazine*, vol. 28, no. 3, pp. 92–112, May 2011.

[13] D. Chen, D. Qu, T. Jiang, and Y. He, "Prototype filter optimization to minimize stopband energy with NPR constraint for filter bank multi-carrier modulation systems," *IEEE Transactions on Signal Processing*, vol. 61, no. 1, pp. 159–169, 2013.

[14] N. Michailow, M. Matthe, I. Gaspar, A. Caldevilla, L. Mendes, A. Festag, and G. Fettweis, "Generalized frequency division multiplexing for 5th generation cellular networks," *IEEE Transactions on Communications*, vol. 62, no. 9, pp. 3045–3061, Sept 2014.

[15] G. Fettweis, M. Krondorf, and S. Bittner, "GFDM - generalized frequency division multiplexing," in *IEEE Vehicular Technology Conference*, April 2009, pp. 1–4.

[16] V. Vakilian, T. Wild, F. Schaich, S. Ten Brink, and J.-F. Frigon, "Universal-filtered multi-carrier technique for wireless systems beyond LTE," in *IEEE Globecom Workshops (GC Wkshps)*, 2013, pp. 223–228.

[17] X. Wang, T. Wild, and F. Schaich, "Filter optimization for carrier-frequency-and timing-offset in universal filtered multi-carrier systems," in *IEEE Vehicular Technology Conference (VTC Spring)*, 2015, pp. 1–6.

[18] J. Abdoli, M. Jia, and J. Ma, "Filtered OFDM: A new waveform for future wireless systems," in *IEEE Signal Processing Advances in Wireless Communications (SPAWC)*, June 2015, pp. 66–70.

[19] F. Schaich and T. Wild, "Waveform contenders for 5G; OFDM vs. FBMC vs. UFMC," in *International Symposium on Communications, Control and Signal Processing (ISCCSP)*, May 2014, pp. 457–460.

[20] J. Li, E. Bala, and R. Yang, "Resource block filtered-OFDM for future spectrally agile and power efficient systems," *Physical Communication*, vol. 11, pp. 36–55, 2014.

[21] H. Lin and P. Siohan, "Multi-carrier modulation analysis and WCP-COQAM proposal," *EURASIP Journal on Advances in Signal Processing*, pp. 1–19, 2014.

[22] A. Aminjavaheri, A. Farhang, A. RezazadehReyhani, and B. Farhang-Boroujeny, "Impact of timing and frequency offsets on multicarrier waveform candidates for 5g," in *IEEE Signal Processing and Signal Processing Education Workshop (SP/SPE)*. IEEE, 2015, pp. 178–183.

[23] X. Yu, Y. Guanghui, Y. Xiao, Y. Zhen, X. Jun, and G. Bo, "FB-OFDM: A novel multicarrier scheme for 5G," in *European Conference on Networks and Communications (EuCNC)*, June 2016, pp. 271–276.

[24] A. Ikhlef and J. Louveaux, "Per subchannel equalization for MIMO FBMC/OQAM systems," in *IEEE Pacific Rim Conference on Communications, Computers and Signal Processing*, Aug 2009, pp. 559–564.

[25] D. Chen, X. G. Xia, T. Jiang, and X. Gao, "Properties and power spectral densities of CP based OQAM-OFDM systems," *IEEE Transactions on Signal Processing*, vol. 63, no. 14, pp. 3561–3575, July 2015.

[26] J. Li, D. Chen, D. Qu, and T. Jiang, "Block-wise alamouti schemes for oqam-ofdm systems with complex orthogonality," *Wireless Communications and Mobile Computing*, September 2016.

[27] L. Zhang, A. Ijaz, P. Xiao, A. Quddus, and R. Tafazolli, "Single-rate and multi-rate multi-service systems for next generation and beyond communications," in *IEEE PIMRC*, Sept. 2016, pp. 1–6.

[28] P. Weitkemper, J. Bazzi, K. Kusume, A. Benjebbour, and Y. Kishiyama, "Adaptive filtered OFDM with regular resource grid," in *2016 IEEE International Conference on Communications Workshops (ICC)*, May 2016, pp. 462–467.
[29] 3GPP TR 36.802, "Narrowband Internet of Things (NB-IoT) – Technical Report for BS and UE radio transmission and reception (Release 13)," Tech. Rep., June 2016.
[30] J. W. Adams, "FIR digital filters with least-squares stopbands subject to peak-gain constraints," *IEEE Transactions on Circuits and Systems*, vol. 38, no. 4, pp. 376–388, Apr 1991.
[31] B. Farhang-Boroujeny, "A square-root nyquist (M) filter design for digital communication systems," *IEEE Transactions on Signal Processing*, vol. 56, no. 5, pp. 2127–2132, May 2008.